The American Journal of Pathology, Vol. 191, No. 6, June 2021

ELSEVIER

The American Journal of PATHOLOGY

ajp.amjpathol.org

VASCULAR BIOLOGY, ATHEROSCLEROSIS, AND ENDOTHELIUM BIOLOGY

Up-Regulation of the Long Noncoding RNA X-Inactive–Specific Transcript and the Sex Bias in Pulmonary Arterial Hypertension

Shanshan Qin,* Dan Predescu,* Brandon Carman,* Priyam Patel,† Jiwang Chen,‡ Miran Kim,§ Tim Lahm,¶ Mark Geraci,|| and Sanda A. Predescu||

From the the Pulmonary, Critical Care and Sleep Medicine, Division of Digestive Diseases and Nutrition,† Department of Internal Medicine, Rush University Medical Center, Chicago, Illinois; Center for Genetic Medicine,‡ Quantitative Data Science Core, Northwestern University Feinberg School of Medicine, Chicago, Illinois; the Division of Pulmonary, Critical Care, Sleep and Allergy,§ Department of Medicine, University of Illinois at Chicago, Chicago, Illinois; the Pulmonary Critical Care Sleep and Occupational Medicine,¶ Indiana University School of Medicine, Indianapolis, Indiana; and the Health Sciences,|| School of Medicine, University of Pittsburgh, Pittsburgh, Pennsylvania*

Accepted for publication March 16, 2021.

Address correspondence to Sanda A. Predescu, Ph.D., Division of Pulmonary, Critical Care and Sleep Medicine, Department of Internal Medicine, Rush University Medical Center, 1750 West Harrison St., Jelke Bldg., 15th Floor, Suite 1535, Chicago, IL 60612. E-mail: Sanda_Predescu@rush.edu.

Pulmonary arterial hypertension (PAH) is a sex-biased disease. Increased expression and activity of the long-noncoding RNA X-inactive–specific transcript (Xist), essential for X-chromosome inactivation and dosage compensation of X-linked genes, may explain the sex bias of PAH. The present studies used a murine model of plexiform PAH, the intersectin-1s (ITSN) heterozygous knockout ($KO^{ITSN+/-}$) mouse transduced with an ITSN fragment (EH_{ITSN}) possessing endothelial cell proliferative activity, in conjunction with molecular, cell biology, biochemical, morphologic, and functional approaches. The data demonstrate significant sex-centered differences with regard to EH_{ITSN}-induced alterations in pulmonary artery remodeling, lung hemodynamics, and p38/ETS domain containing protein/c-Fos signaling, altogether leading to a more severe female lung PAH phenotype. Moreover, the long-noncoding RNA—Xist is up-regulated in the lungs of female EH_{ITSN}-$KO^{ITSN+/-}$ mice compared with that in female wild-type mice, leading to sex-specific modulation of the X-linked gene ETS domain containing protein and its target, two molecular events also characteristic to female human PAH lung. More importantly, cyclin A1 expression in the S and G_2/M phases of the cell cycle of synchronized pulmonary artery endothelial cells of female PAH patients is greater versus controls, suggesting functional hyperproliferation. Thus, Xist up-regulation leading to female pulmonary artery endothelial cell sexual dimorphic behavior may provide a better understanding of the origin of sex bias in PAH. Notably, the EH_{ITSN}-$KO^{ITSN+/-}$ mouse is a unique experimental animal model of PAH that recapitulates most of the sexually dimorphic characteristics of human disease. *(Am J Pathol 2021, 191: 1135–1150; https://doi.org/10.1016/j.ajpath.2021.03.009)*

Pulmonary arterial hypertension (PAH) is a pulmonary vasculopathy with a 3-year survival rate of only 55%. Recent population-based studies indicate a female predominance in PAH of around two to four over men for all races and ethnicities and across all ages studied to date, except for HIV-associated and portopulmonary hypertension, which tend to occur more often in men.[1] Although female sex has long been established as the major clinical risk factor for PAH, male sex doubles the risk of death in PAH.[2] Even if sex is the strongest disease modifier known, the female predominance in PAH incidence remains largely unexplained. PAH is thought to develop in response to a genetic abnormality and an environmental insult that triggers endothelial cell (EC) apoptosis, abnormal vascular remodeling, and loss of small distal vessels, leading to increased pulmonary vascular

Supported by NIH R01 HL127022 (S.P.), NIH 1R01HL144727-01A1, and Veterans Affairs Merit Review Award 2 I01 BX002042 (T.L.). Funding for the Pulmonary Hypertension Breakthrough Initiative is provided under National Heart, Lung, and Blood Institute R24 grant R24HL123767 and by the Cardiovascular Medical Research and Education Fund.

Disclosures: None declared.

https://doi.org/10.1016/j.ajpath.2021.03.009

resistance and reduced blood flow.[3] Female sex hormones, primarily estrogens, may play a causative role in the development of PAH.[4] The estrogen paradox of increased female susceptibility in PAH, but longer life than males after diagnosis of PAH, remains unexplained.[5] Estrogens have been uniformly shown to be cardioprotective in the right ventricle (RV), vasculature they may exert disease-promoting effects in the pulmonary vasculature.[2] Moreover, the effects of estrogens and their metabolites in animal studies show differences compared with epidemiologic studies in humans.[6] Although estrogens have been found to be protective in various experimental models of PAH, the registry data demonstrate a consistent female susceptibility to the disease. Despite the strong female sex bias observed in idiopathic and familial PAH patients, commonly used animal models of PAH puzzlingly show increased male susceptibility.[6] It is still unclear why estrogens appear to be protective in certain models [ie, hypoxia- and monocrotaline-induced pulmonary hypertension and Sugen5416 (the vascular endothelial growth factor [VEGF] receptor 2) inhibitor/hypoxia (Su/Hx) rat] and detrimental in others (ie, mice overexpressing serotonin transporter and mice overexpressing the calcium-binding protein metastasis-associated S100A4/Mts1[7,8]). Lack of experimental animal models of PAH that more closely mimic the vascular changes in human PAH may explain this lack of consistency.

Accumulating evidence indicates that epigenetic alterations such as DNA methylation, chromatin remodeling, and gene imprinting, as well as long-noncoding RNA (lncRNA) regulation play key roles in the development and progression of many human diseases.[9] LncRNAs are involved in many aspects of gene regulation, including epigenetic regulation, imprinting, trafficking between the nucleus and cytoplasm, transcription, and mRNA splicing.[9] Recent studies demonstrate that the X-inactive−specific transcript (XIST/Xist), one of the first lncRNAs discovered in mammals, is an abnormally expressed lncRNA in several cancers, which negatively relates to clinical outcome; and its abnormal expression may partially contribute to disease sex bias.[9] In mammals, equal dosage of X-linked genes between the sexes is ensured through the process of X-chromosome (X-Chr) inactivation.[10] Previous studies have established that X-Chr inactivation is mediated by the lncRNA-Xist.[11,12] Abnormal Xist interferes with the expression profiles of the X-linked genes, and is related to tumorigenesis, cell cycle, apoptosis, and cell proliferation. This is relevant, as abnormal Xist expression may result in aberrant expression of the X-linked genes (ie, *apelin*,[13−15] *tissue inhibitor of metalloproteinase-1*,[16−18] *histone deacetylase 6*,[19] *angiotensin-converting enzyme 2*,[20,21] *filamin*,[22,23] *O-linked β-N-acetyl-glucosamine*,[24] *host cell factor-1*,[24] *androgen receptor*,[25] *NADP oxidase*,[26,27] and *ETS domain containing protein* [*Elk1*][28]) involved in PAH pathogenesis.[29] Although significant progress has been made recently in understanding the effects of sex hormones on RV function, a critical determinant of survival in PAH,[8,30] no studies have addressed the effects of the lncRNA-Xist on EC proliferative/plexiform phenotype.

The mouse model of plexogenic PAH, recently generated via a two-hit pathophysiological mechanism without hypoxia,[28] characterized by intersectin-1s (ITSN) deficiency and prolonged lung expression of the EH_{ITSN}, develops a severe lung phenotype characterized by occlusive proliferation of ECs and formation of plexiform lesions as well as differences in RV function. EH_{ITSN} is an ITSN fragment with EC proliferative potential present in the lungs of PAH animal models and human patients.[28,31] Moreover, recent studies have shown that human pulmonary artery endothelial cells (PAECs) are sex dimorphic in their proliferative potential.[29] In response to the EH_{ITSN} expression, the female PAECs show significant up-regulation of the lncRNA-Xist compared with EH_{ITSN}-transfected male PAECs as well as to non-transfected cells. This accounts, at least in part, for their increased proliferation in response to the EH_{ITSN}. The aims of this study were to determine whether sex differences exist in the EH_{ITSN}-transduced $ITSN^{+/-}$ mice and whether the lncRNA-Xist contributes to the mouse PAH lung phenotype. The findings demonstrate that the lncRNA-Xist, essential for X-Chr inactivation and dosage compensation of X-linked genes, is substantially overexpressed in female EH_{ITSN}-$KO^{ITSN+/-}$ mouse lungs in comparison with wild-type (wt) female mice. This leads to sex-specific modulation of one of the X-Chr−linked PAH genes, the Elk1 transcription factor,[32,33] and of cyclin A1, Elk1 target, and a cell cycle regulatory protein.[34,35] These molecular events are more prominent in female mouse EH_{ITSN}-$KO^{ITSN+/-}$ PAH model compared with those in males. Moreover, the expression of Elk1 and cyclin A1 also shows a sex-specific regulation in the lung specimens of female human PAH patients. Thus, these studies demonstrate that the EH_{ITSN}-$KO^{ITSN+/-}$ mouse model of plexiform arteriopathy recapitulates several sex-specific differences of human disease. Moreover, the studies strongly suggest that lncRNA-Xist up-regulation accounts for female PAEC sexual dimorphism in the proliferative response and may provide possible new targets for drug development against plexiform arteriopathy in female patients.

Materials and Methods

The reagents were obtained as follows: cholesterol (catalog number PHR1533), dimethyl dioctadecyl ammonium bromide (catalog number S234850), hydrogen peroxide (catalog number H1009), glycerol (catalog number G5516), benzamidine (catalog number 434760), phenylmethylsulfonyl fluoride (catalog number P7626), sodium pyrophosphate, bovine serum albumin, desipramine hydrochloride (catalog number D3900), protease inhibitor cocktail (catalog number P8340), poly-lysine solution (catalog number P8920) tissue culture grade, and Hank's solution from Sigma-Aldrich (St. Louis, MO); micro bicinchoninic acid protein assay kit (catalog number 23235) and enhanced chemiluminescent substrate (catalog number 34080) from Pierce (Rockford, IL); Triton X-100 (catalog number

T8787), SDS (catalog number 15525017), Tween-20 (catalog number 85115), nitrocellulose membranes (catalog number 1629997), and all reagents for electrophoresis from ThermoFisher Scientific (Rockford, IL); and ProLong Antifade reagent (catalog number P-36984) from Molecular Probes, Eugene, OR. The polycarbonate 50-nm filters (catalog number LF M50) and the mini extruder were from Avestin, Inc. (Ottawa, ON, Canada). The following primary antibodies (Abs) were used: rabbit anti-actin monoclonal Ab (catalog number A-3853) from Sigma-Aldrich; phosphorylated p38 monoclonal Ab (catalog number 4511) and c-Fos polyclonal Ab (catalog number 4384) from Cell Signaling Technology (Beverly, MA); and Elk1 polyclonal Ab (catalog number sc-365876) from Santa Cruz Biotechnology (Dallas, TX). Horseradish peroxidase–conjugated reporter Abs were from Cappel, Organon Teknika (Durham, NC). TransAM Kit (catalog number 44396), for Elk1 activation, was from Active Motif (Carlsbad, CA); and the NE-PER Nuclear and Cytoplasmic Extraction kit (catalog number 78833) from Pierce.

$KO^{ITSN+/-}$ mice, strain 129SV/J genetic background, were kindly provided by Dr. Melanie Pritchard (Monash University, Clayton, Australia). Breeding colonies were maintained in the Rush University (Chicago, IL) animal facility. RNA samples of human failed donors (FDs) and PAH lung tissue were provided by the Pulmonary Hypertension Breakthrough Initiative. Lung tissue of rats subjected to Su/Hx exposure, as the study by Frump et al,[8] were kindly provided by Dr. Tim Lahm (Indiana University, Indianapolis, IN). Male and female idiopathic pulmonary artery endothelial cells of pulmonary arterial hypertension patients ($PAEC_{PAH}$) and of nondisease controls were from the Pulmonary Hypertension Breakthrough Initiative or kindly provided by Drs. Serpil Erzurum and Suzy Comhair (Lerner Research Institute, Cleveland Clinic, Cleveland, OH), passages 3 to 5. The PAECs were harvested and cultured, as described previously.[36] The PAECs were de-identified in accordance with the Health Insurance Portability and Accountability Act and authenticated to confirm their endothelial identity. The studies were conducted in compliance with the Pulmonary Hypertension Breakthrough Initiative guidelines, as per material transfer agreement. The studies do not meet the definition of human subject research (15090702-IRB02-CR04).

Animal Studies

All animal (rodent) studies were performed according to the guidelines of Rush University Institutional Animal Care and Use Committee. $KO^{ITSN+/-}$ mice, 129SV/J genetic background, were kindly provided by Dr. Melanie Pritchard. Breeding colonies were maintained in the Rush University animal facility. All mice, 12 to 16 weeks old, 20 g to 30 g, were kept under standardized housing and feeding conditions. All experiments were done under anesthesia using ketamine (60 mg/kg) and acepromazine (2.5 mg/kg) + xylazine (2.5 mg/kg), in 0.1 to 0.2 mL sterile phosphate-buffered saline. Mice were genotyped by tail snipping standard procedure.[28] All experiments were repeated at least three times. No mouse mortality occurred during the study. In addition, all studies using rodents adhered to American Physiological Society's Guiding Principles in the Care and Use of Vertebrate Animals in Research and Training and were performed according with the Rush University Institutional Animal Care and Use Committee approved protocol.

Myc-EH_{ITSN} DNA (amino acids 1 to 271), cloned into the pReceiver/myc-M43 vector, was delivered to mouse lungs via cationic liposomes, as described previously.[37] DNA-liposome complexes were prepared at a ratio of 8 nmol liposomes:1 μg myc-EH_{ITSN} DNA, a ratio found in previous studies to induce efficient protein expression without pulmonary toxicity.[38,39] Long-term myc-EH_{ITS} protein expression was achieved by repeated myc-EH_{ITSN} DNA-liposome delivery, every 48 hours for 18 days. A mutant $EH_{ITSN\text{-}W263A}$ fragment, in which the Trp (W) 263 was substituted with Ala [(A), a substitution that reduces NPF (Asn-Pro-Phe), the main target of the EH domain binding, beyond detection[40]] was cloned into the same vector and used as control. At the end of the treatment period, mice were anesthetized by i.p. delivery of 1 mL/kg body weight (BW) of ketamine hydrochloride/xylazine hydrochloride solution (Sigma-Aldrich). Hemodynamic measurements and tissue harvesting for histology, morphometric, molecular biology, and biochemical analyses were performed. Mice were divided in three groups, males and females: group 1, EH_{ITSN}-transduced $KO^{ITSN+/-}$; group 2, untreated $KO^{ITSN+/-}$; and group 3, wt mice. Age- and BW-matched mice were used.

Lung Histology

Mouse lungs were inflated with 1% low-melting point agarose in 10% formalin at a constant pressure of 25 cm H_2O, allowing for homogeneous expansion of lung parenchyma, and then fixed in 4% paraformaldehyde for 48 hours and paraffin-embedded.[38] Thin sections (4 to 5 μm thick), cut longitudinally, were stained with hematoxylin/eosin. Images were acquired with a 20× lens using a Zeiss (Thornwood, NY) AxioImagerM1 microscope equipped with a color digital camera.

Hemodynamic Measurement; Echocardiography

For the hemodynamic measurements in mice, a Millar system, which includes a microtip catheter transducer (model PVR-1030), pressure volume system, and Power Lab Data (Houston, TX) acquisition system using Lab Chart Pro 7.0 software, has been employed. The catheter was inserted into the RV via the external right jugular vein. The Fulton index (the ratio of RV weight to left ventricle + septum weight) or RV weight relative to the animal's BW was determined as a measurement for RV hypertrophy. Echocardiography was

performed at the University of Illinois at Chicago, Small Animal Physiology Core. Briefly, mice were anesthetized using inhaled isoflurane via a facemask and then subjected to transthoracic echocardiography using VisualSonics Vevo 2100 (VisualSonics Inc., Toronto, ON, Canada) and a MS-550D, 22- to 55-MHz mouse transducer. Pulse-wave Doppler echocardiography was used to record the pulmonary blood outflow at the level of the aortic valve in the short-axis view to measure pulmonary acceleration time (PAT) values. All measurements were averaged on five cardiac cycles. At the end of each experiment, the heart was excised from the thoracic cavity, the atria were removed, and the RV free wall was separated from the left ventricle, including the septum. Tissues were blotted and weighted. The ratio RV/BW and the Fulton ratio [RV/(left ventricle + septum] were calculated.

Morphometric Analysis

For assessment of the extent of pulmonary vascular remodeling, a stereological assessment of the intima + media thickness on 30 slides for every lung has been conducted. The stereological Stepanizer software version β 2.28 (*http://www.stepanizer.com*, last accessed January 19, 2019)[41] was used, with a 1024-point grid (for assessment of pulmonary artery area) and subsampling with a 16-point (course) grid for assessment of alveolar septa, as described previously.[42] The thickness of pulmonary arteries was determined on the basis of sum of point hits in pulmonary artery (intima + media) per 50 histologic fields. The number of profiles of plexiform lesions per slide was determined by the identification of lesion profiles with the characteristics described in human PAH patients[43,44] and Su/Hx rat model of PAH.[45] Uncertain plexiform lesions were not considered for final count. Quantification of affected vessels was performed on small and medium-sized blood vessels (20 μm $\geq$ diameter $\leq$ 100 μm), as above, using three sections/mouse, three mice, males and females each, in the control group and five male and five female, in the experimental group, with the experiments performed at least three times with reproducible results. This number of mice was considered sufficient to detect relevant differences when significance is set at $P < 0.05$.

RNA Sequencing

RNA from human PAECs and mouse lung was isolated with RNeasy Micro Kit (Qiagen, Valencia, CA). The quality of DNA reads, in FASTQ format, was evaluated using FastQC. Adapters were trimmed, and reads of poor quality or aligning to rRNA sequences were filtered using Trim Galore (*http://www.bioinformatics.babraham.ac.uk/projects/trim_galore*, last accessed March 18, 2021). The cleaned reads were aligned to the human genome (hg19) using STAR.[46] Read counts for each gene were calculated using HTSeq-Counts,[47] in conjunction with a gene annotation file for hg19 obtained from University of California, Santa Cruz (*http://genome.ucsc.edu*, last accessed March 18, 2021). A comprehensive quality control report was generated using MultiQC.[48] Differential expression was determined using DESeq2.[49] The cutoff for determining significantly differentially expressed genes was a false discovery rate−adjusted $P < 0.05$. The pathway analysis was done using Metascape.[50]

Protein Extraction and Western Blot Analysis

Mouse lung tissue was homogenized in a buffer containing 20 mmol/L Tris-HCl, pH 7.4, 150 mmol/L NaCl, 1 mmol/L phenylmethylsulfonyl fluoride, and protease and phosphatase inhibitors, using a Brinkmann Polytron homogenizer (KINEMATICA AG, CH-6014 Littau, Luzern, Switzerland). Total lung lysates were prepared by adding SDS and Triton X-100 to a final concentration of 0.3% and 1%, respectively, for 2 hours, at 4°C. The resulting lysates were clarified by centrifugation in a Beckman Optima Max-XP ultracentrifuge (Beckman Coulter, Indianapolis, IN) with a TLA-55 rotor at 124,500 × g for 45 minutes at 4°C. Protein concentration was determined using the micro bicinchoninic acid protein assay with bovine serum albumin standard. Protein samples normalized for total protein were subjected to SDS-PAGE and transferred to nitrocellulose membranes. Strips of nitrocellulose membranes were incubated with the primary and reporter Abs and processed, as described previously.[37] The reaction was visualized using the enhanced chemiluminescent substrate kit. The primary Abs were diluted 1:500 (Elk-1), 1:1000 (phosphorylated p38 and c-Fos), and 1:2000 (actin) using 5% Blotto (Rockland, Limerick, PA) in Tris-buffered saline. Horseradish peroxidase−conjugated reporter Abs were used at 1:1000 dilution. X-ray films were subjected to densitometry using the ImageJ software version 2.0 (NIH, Bethesda, MD; *https://imagej.nih.gov/ij*, last accessed February 24, 2021).

RNA Isolation and qPCR

Real-time quantitative PCR (qPCR) was performed on cDNA generated from 2000 ng of total RNA using High-Capacity RNA-to-cDNA Kit and Power SYBR Green PCR Master Mix (catalog number 12004176; Thermo Fisher Scientific, Hanover Park, IL). Amplification and detection of specific products were performed with a Roche Light Cycler 480 Detection System (Indianapolis, IN). Relative gene expression was calculated by comparing cycle times for each target PCR. The primers' forward and reverse sequences, as well as the catalog numbers for rat and mouse lncRNA-Xist and human Elk1 (Sigma-Aldrich), mouse and human glyceraldehyde-3-phosphate dehydrogenase and mouse Elk1 (Origene, Rockville, MD), rat Elk1, mouse and rat cyclin A1, rat glyceraldehyde-3-phosphate dehydrogenase (Gene Copoeia, Inc., Rockville MD), and human lncRNA Xist (BioRad, Hercules, CA) are included in

Table 1 The Primer Forward and Reverse Sequences for lncRNA-Xist and Human Elk1 (Sigma-Aldrich), Mouse and Human GAPDH and Mouse Elk1 (Origene), Rat Elk1, Mouse and Rat Cyclin A1, and Rat GAPDH (Gene Copoeia, Inc.), and Human lncRNA Xist (BioRad), Used for qPCR Analysis

Oligonucleotide name (catalog no.)	Forward sequence	Reverse sequence
lncRNA Xist (rat)	5′-TGCCTGGATTTAGAGGAG-3′	5′-CTCCACCTAGGGATCGTAA-3′
	Oligonucleotide no. 3023101015—000030	Oligonucleotide no. 3023101015—000040
lncRNA Xist (mouse)	5′-GCCCAAAGGGACAAACAATC-3′	5′-GTAGCGAGGACTTGAAGAGAAG-3′
	Oligonucleotide no. 3022576202—000010	Oligonucleotide no. 3022576202—000020
lncRNA Xist (human) (catalog no. 12004176)	5′-GGATGTCAAAAGATCGGCCC-3′	5′-GTCCTCAGGTCTCACATGCT-3′
Elk1 (rat) (catalog no. RQP067189)	5′-GGCTTCAGTCCAGAAGCTGT-3′	5′-GGGGTTGGGTGATCTCAGTG-3′
Elk1 (mouse) (catalog no. MP204140)	5′-GGAACAAGCTCTGGTCTTCAGG-3′	5′-GGACTCAGAGTGCTCCAGAAATG-3′
Elk1 (human)	5′-GCTGCCTCCTAGCATTCACTTC-3′	5′-CCACGCTGATAGAAGGGATGTG-3′
	Oligonucleotide no. 3022585344—000130	Oligonucleotide no. 3022585344000140
Cyclin A1 (rat) (catalog no. RQP046089)	5′-ACCGTGCTAGGAGTGTTGAC-3′	5′-CCAGCTGCAGGGAAGACATT-3′
Cyclin A1 (mouse) (catalog no. 026720MQP)	5′-TGAGCCTTCTGGAAGCTGAC-3′	5′-ACTCAGGCAAGGCACAATCT-3′
GAPDH (rat) (catalog no. RQP049537)	5′-CAGCCGCATCTTCTTGTGC-3′	5′-GGTAACCAGGCGTCCGATA-3′
GAPDH (mouse) (catalog no. MP205604)	5′-CATCACTGCCACCCAGAAGACTG-3′	5′-ATGCCAGTGAGCTTCCCGTTCAG-3′
GAPDH (human) (catalog no. HP205798)	5′-GTCTCCTCTGACTTCAACAGCG-3′	5′-ACCAACCCTGTTGCTGTAGCCAA-3′

Elk1, ETS domain containing protein; GAPDH, glyceraldehyde-3-phosphate dehydrogenase; lncRNA, long noncoding RNA; qPCR, real-time quantitative PCR.

Table 1. Glyceraldehyde-3-phosphate dehydrogenase sequences were used as internal control, for mRNA normalization. PCRs were run under following conditions: 95°C for 10 minutes; 95°C for 15 seconds + 60°C for 1 minute, repeated 40 times; and the melting curve was 95°C for 15 seconds + 60°C for 1 minute + 95°C for 15 seconds. Once the fluorescent signals were normalized to an internal reference, the C_T was set within the exponential phase of the reaction, the relative gene expression was assessed as ΔC_T value, and the comparative expression between treatments was subsequently calculated using the following equation: relative gene expression $= 2_T^{-(\Delta C\ \text{sample} - \Delta C\ \text{control})}$.

Elk-1 Transcription Factor Assay

Nuclear extracts of controls and EH_{ITSN}-transduced mice were prepared using the NE-PER Nuclear and Cytoplasmic Extraction kit, as previously described.[37] The nuclear extracts were analyzed by enzyme-linked immunosorbent assay using the TransAM Kit with colorimetric readout quantifiable by spectrophotometry, in a 96-well plate containing the immobilized Elk-1 consensus site oligonucleotide. Activated Elk-1 was detected via an Ab against phosphorylated Elk-1, followed by a horseradish peroxidase—conjugated reporter Ab. The plates were read at 450 nm using an Epoch plate reader (BioTek, Winooski, VT).

Statistical Analysis

For comparison of two groups, *t*-tests (two tailed) were performed using the GraphPad Prism 8.0 software (Graph Pad Software, San Diego, CA). All data are shown as means ± SD. A value of $P < 0.05$ was considered significant.

Results

The EH_{ITSN}-Induced Mouse Model of PAH Recapitulates Most of the Sex Differences of Human Disease

The recently developed mouse model of plexogenic PAH generated via a two-hit pathophysiological mechanism without hypoxia[28] was used to investigate sex differences in the lung phenotype, similar to human disease. ITSN knockout/heterozygous ($KO^{ITSN+/-}$) mice were transduced via cationic liposomes with an ITSN fragment possessing EC proliferative activity (EH_{ITSN}), as described previously.[28] The EH_{ITSN} is a result of granzyme B cleavage of ITSN under inflammatory conditions associated with PAH and is present in the lungs of PAH animal models and human patients.[28,37] Morphologic and morphometric analyses of lung tissue sections indicated that the EH_{ITSN}-$KO^{ITSN+/-}$ female mice show a more severe PAH phenotype compared with EH_{ITSN}-$KO^{ITSN+/-}$ male mice.

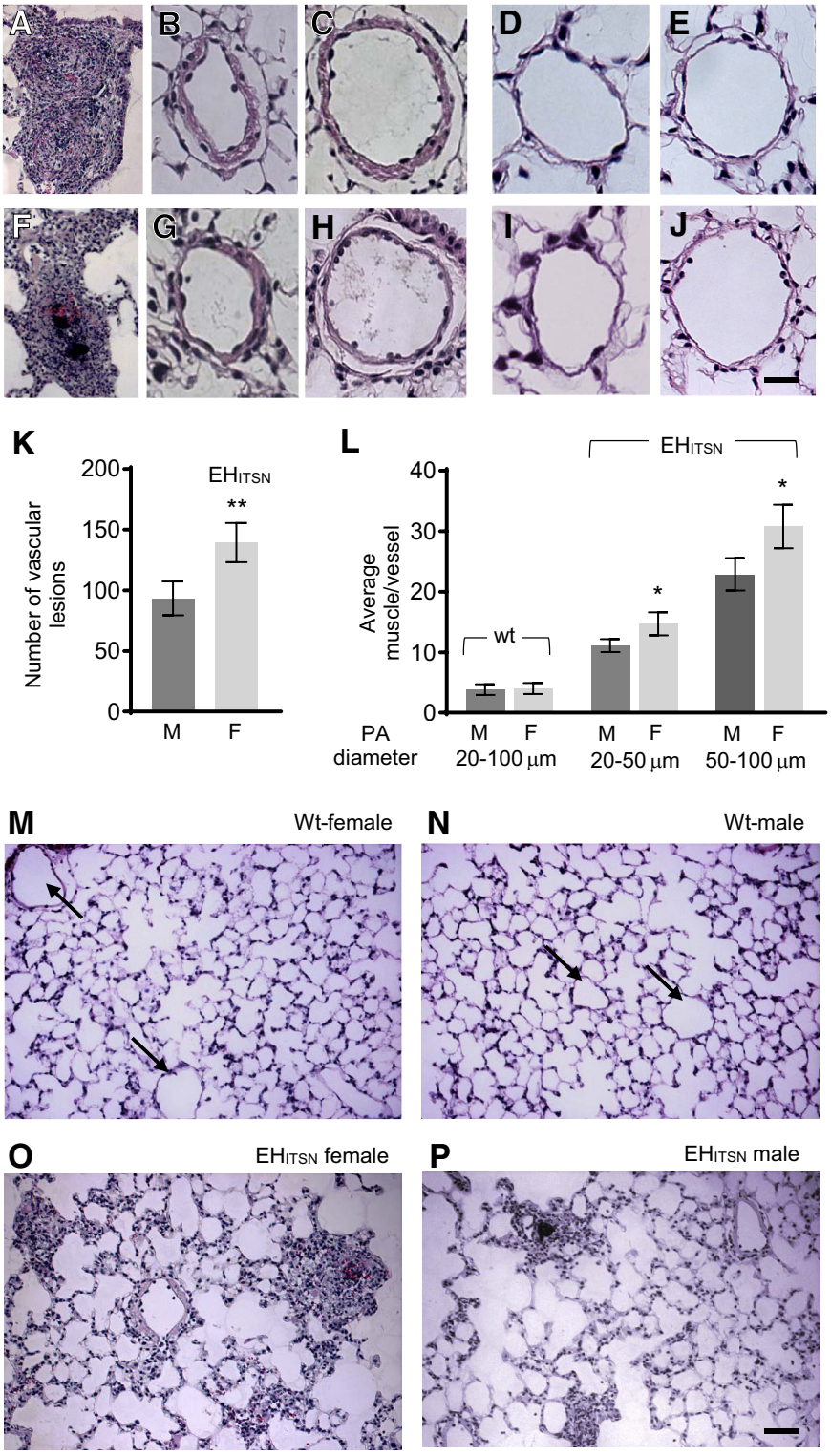

Figure 1 EH_{ITSN} induces significant differences in pulmonary artery remodeling between female (F) and male (M) EH_{ITSN}-$KO^{ITSN+/-}$ mice. Representative hematoxylin/eosin staining of mouse lung sections illustrates the vascular arteriopathy and pulmonary artery (PA), different diameter, remodeling in female (**A**–**C**) and male (**F**–**H**) EH_{ITSN}-$KO^{ITSN+/-}$ mice. Lung sections of wild-type (wt) female (**D** and **E**) and male (**I** and **J**) mice illustrate representative pulmonary arteries of different diameter used for comparison. Quantification of vascular lesions (**K**) and morphometric analyses of small (20 to 50 μm) and medium (50 to 100 μm) pulmonary artery muscularization in wt female and wt male mice, as well as in female and male EH_{ITSN}-$KO^{ITSN+/-}$ mice (**L**). The morphometric analyses of small and medium pulmonary artery muscularization for wt male and wt female mice show aggregated (20 to 100 μm diameter) data. The number of lesions is reported per three mouse lung cross-sections. Low magnifications of the lung images, female and male wt mice (**M** and **N**) and EH_{ITSN}-$KO^{ITSN+/-}$ mice (**O** and **P**), are also shown. **Arrows** (**M** and **N**) indicate vascular profiles. $n = 3$ mice for each wt male and wt female data (**D, E, I, J, M**, and **N**); $n = 9$ mice for each female and male, with 3 slides per mouse, per experimental condition (**A**–**C, F**–**H, O**, and **P**). $^{*}P < 0.05$, $^{**}P < 0.01$. Scale bars: 20 μm (**A**–**J**); 40 μm (**M**–**P**). Original magnification, ×20 (**M**–**P**).

Specifically, the data indicate 37.5% more occlusive lesions (including complex plexiform lesions) per lung cross-section (Figure 1, A, F, and K) and approximately 22% more muscularization of the small (20 to 50 μm) pulmonary arteries (Figure 1, B, G, and L) and medium-sized (51 to 100 μm) pulmonary arteries (Figure 1, C, H, and L). Medial thickening was significantly higher in the EH_{ITSN}-transduced $KO^{ITSN+/-}$ female mice as compared to EH_{ITSN}-$KO^{ITSN+/-}$ male mice. More importantly, the occlusive lesions, including plexiform lesions, were larger and with a higher complexity in the lungs of female mice compared with those in males. Small and medium-sized pulmonary

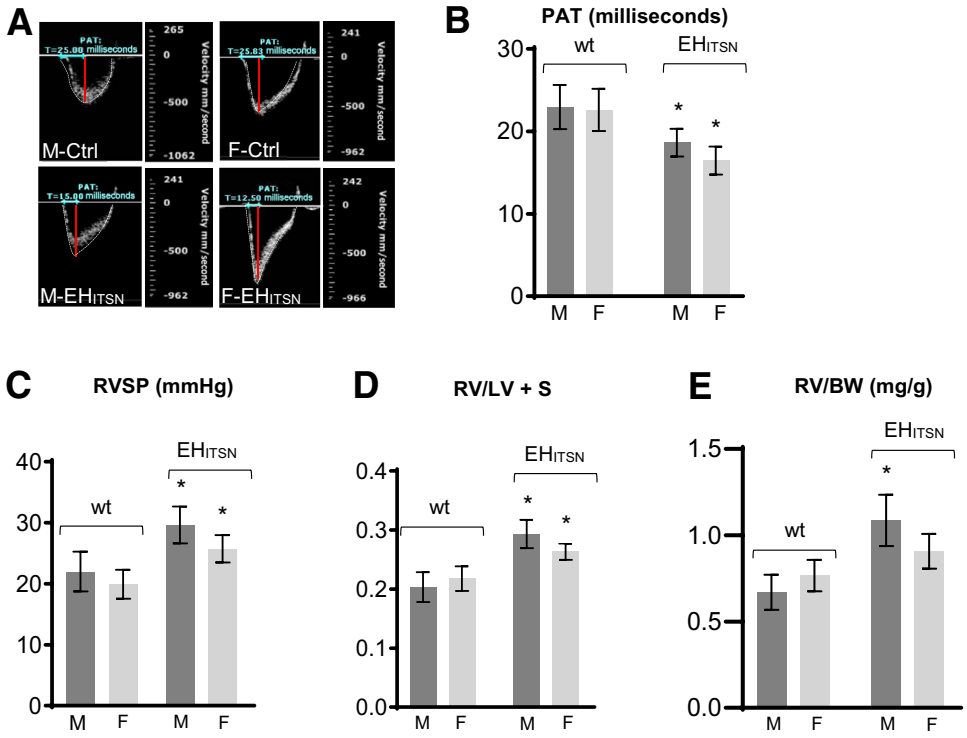

Figure 2 **A:** EH_{ITSN} induces significant differences in pulmonary blood flow, right ventricular systolic pressure (RVSP), and right ventricular (RV) hypertrophy between female (F) and male (M) EH_{ITSN}-$KO^{ITSN+/-}$ mice. Representative pulsed-wave Doppler echocardiography (ECHO) recordings of the pulmonary artery blood flow in wild-type (wt) and EH_{ITSN}-$KO^{ITSN+/-}$ mice, males and females; images are taken from the pulsed-wave Doppler tracings. **B:** Average pulmonary acceleration time (PAT) values in wt and EH_{ITSN}-$KO^{ITSN+/-}$ mice, estimated from the ECHO measurements. **C** and **D:** RVSP values (**C**) and RV hypertrophy (**D**), measured as the RV/left ventricle (LV) + septum (S) weight ratio (Fulton index) in male and female EH_{ITSN}-$KO^{ITSN+/-}$ mice. **E:** RV/body weight (BW) ratio (mg/g) in male and female EH_{ITSN}-$KO^{ITSN+/-}$ mice. Data are shown as means ± SD (**B**–**E**). $n = 3$ independent experiments, with 7 to 9 mice per experimental condition (**B**–**E**). *$P < 0.05$ for F-EH_{ITSN} and M-EH_{ITSN} versus their corresponding, wt F and wt M mice, used as controls (Ctrl).

arteries of wt controls, female (Figure 1, D and E) and male (Figure 1, I and J) mice (129SV/J genetic background), were used for comparison. Low magnifications (×20) of the lung images, female and male wt mice showing small blood vessels with no vascular lesions or remodeling (Figure 1, M and N) and EH_{ITSN}-$KO^{ITSN+/-}$ mice (Figure 1, O and P), are also presented.

Next, PAT measurements were performed (Figure 2A). PAT, defined as the time from the onset of flow to peak velocity by pulse-wave Doppler recording, is a useful index of pulmonary artery pressure in mice. At baseline, in wt mice, the pulmonary systolic flow pattern was relatively symmetric (Figure 2A) in male-Ctrl and female-Ctrl mice. EH_{ITSN} expression progressively shifted the peak of the Doppler flow pattern toward early systole, reflecting a decrease in the PAT and resulting in an asymmetric pattern (Figure 2A) in male-EH_{ITSN} and female-EH_{ITSN} mice. Echocardiography to measure PAT indicated similar values for male and female wt mice (23.67 ± 0.54 milliseconds in male mice and 22.92 ± 0.56 milliseconds in female mice) at baseline. Although EH_{ITSN} lowered PAT values in both male and female EH_{ITSN}-$KO^{ITSN+/-}$ mice, the female mice had 13% lower values (16.41 ± 0.53 versus 18.62 ± 0.58 milliseconds) than male mice (Figure 2B). Consistent with the gendered paradox in PAH, EH_{ITSN}-$KO^{ITSN+/-}$ male mice exhibit higher right ventricular systolic pressure (RVSP) values. In the present study, the EH_{ITSN}-$KO^{ITSN+/-}$ male mice, 129SV/J genetic background, had an RVSP of 29.75 ± 2.5 mm Hg, whereas female EH_{ITSN}-$KO^{ITSN+/-}$ mice had a value of 23.88 mm Hg (Figure 2C). Elevated RVSP was defined as RVSP above the means + 2 SDs of the normal values (20.78 mm Hg). In severe PAH, the RV increases in size in response to volume and pressure overload. The Fulton index, indicative of RV hypertrophy, showed significant increase in both male and female EH_{ITSN}-$KO^{ITSN+/-}$ mice compared with the wt male and female mice; however, with less drastic differences (0.279 ± 0.06 in male and 0.262 ± 0.07 in female EH_{ITSN}-$KO^{ITSN+/-}$ mice) (Figure 2D). Finally, the worse RV function in male EH_{ITSN}-$KO^{ITSN+/-}$ mice was reflected by the RV/BW ratio (Figure 2E). RV mass was slightly higher in the wt female mice. However, in the EH_{ITSN}-$KO^{ITSN+/-}$ male mice, the RV/BW (mg/g) ratio was 20% greater, consistent with observations in human male patients who have worse RV function compared to females, despite similar afterload.[51]

Subsequent studies were designed to analyze the activation of p38/Elk1/c-Fos signaling pathway, which accounts for EC proliferation and formation of plexiform lesions in this murine model of PAH.[28] Biochemical studies of

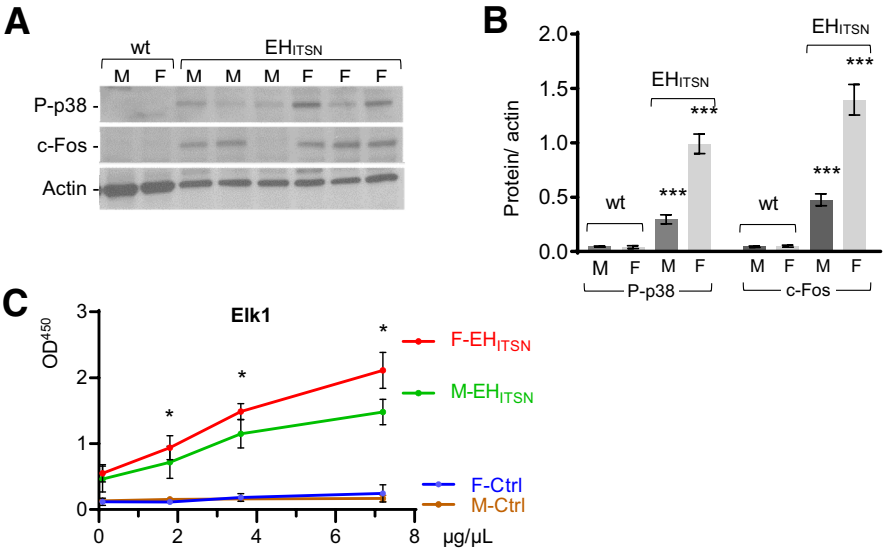

Figure 3 Augmented p38^{MAPK}/Elk1/c-Fos signaling in the lungs of female EH_{ITSN}-$KO^{ITSN+/-}$ mice. **A:** Representative Western blot of lung (70 μg per lane) and nuclear (45 μg per lane) extracts of wild-type (wt) and EH_{ITSN}-$KO^{ITSN+/-}$ male (M) and female (F) mice, for p38^{MAPK} phosphorylation and c-Fos expression, as indicated. Actin served as loading control. **B:** Data of densitometry analyses are shown as protein/actin ratio and are representative for three independent experiments, with three to five mice, each sex, per experiment. **C:** Nuclear extracts of male and female wt and EH_{ITSN}-$KO^{ITSN+/-}$ mouse lungs were assayed for Elk1 activity. Data are representative of three independent triplicate experiments with three mice, each sex, per experiment. Data represent means ± SD (**B** and **C**). $*P < 0.05$ for F-EH_{ITSN} versus M-EH_{ITSN}; $***P < 0.001$ for M-EH_{ITSN} and F-EH_{ITSN} versus corresponding male and female wt mice. Ctrl, control; Elk1, ETS domain containing protein; P-p38, phosphorylated p38.

EH_{ITSN}-$KO^{ITSN+/-}$ mouse lung lysates and nuclear extracts revealed that the extent of p38^{MAPK} activation and up-regulation of the c-Fos immediate early response gene expression were greater in the female EH_{ITSN}-$KO^{ITSN+/-}$ mice compared with those in males (Figure 3, A and B). Likewise, Elk1 transcription factor activation was greater in the female EH_{ITSN}-$KO^{ITSN+/-}$ mice compared with that in males (Figure 3C) and correlates with the degree of plexiform arteriopathy and severity of PAH phenotype (data not shown). Since the EH_{ITSN}-$KO^{ITSN+/-}$ mouse model of PAH recapitulates most of the sex-specific differences of human disease, with female mice developing a more severe PAH phenotype compared with male mice, this murine model is suitable to study the genetics of sex differences in PAH.

Expression of the EH_{ITSN} in the Lung Endothelium of EH_{ITSN}-$KO^{ITSN+/-}$ Murine Model of Plexiform PAH Up-Regulates the Expression of the lncRNA-Xist in Female

The female PAECs, either stably transfected with EH_{ITSN} or from human PAH patients, show significant up-regulation and increased transcriptional activity of the lncRNA-Xist compared with female baseline healthy state.[32] The levels of Xist expression were analyzed in the mouse lung samples by qPCR (Figure 4A). The lncRNA-Xist is up-regulated in the lungs of female EH_{ITSN}-$KO^{ITSN+/-}$ mice compared with that in female wt mice. A 1.2-fold increase in Xist level was detected in female EH_{ITSN}-$KO^{ITSN+/-}$ versus female wt mice, whereas the male EH_{ITSN}-$KO^{ITSN+/-}$ mice show insignificant increase. The qPCR analysis was extended to the lung tissue of Su/Hx rats, a widely used and generally accepted animal model of PAH that develops severe plexiform arteriopathy.[45] No significant differences were observed between female and male with regard to Su/Hx-induced alterations in the RVSP, RV hypertrophy, or pulmonary artery remodeling.[8] The female Su/Hx rats showed no change in Xist expression versus female wt rats, whereas the male Su/Hx rats showed <30% decrease in Xist expression versus the male wt rats (Figure 4B). To increase the clinical relevance of the study, qPCR was performed on total RNA isolated from human male and female PAH lung tissue (Figure 4C). All female PAH specimens showed Xist up-regulation (1.85-fold increase in female PAH versus FD), whereas male PAH specimens showed a wide range of values, with an average of 1.3-fold increase (not significant) versus FD samples. Altogether, these findings further suggest that the increase in Xist expression in the EH_{ITSN}-$KO^{ITSN+/-}$ female mice and human PAH female specimens may account for the sex differences in this sex-biased disease.

Murine PAECs Show Sex Differences in the Proliferative Response to the EH_{ITSN} Expression

As the recent studies indicate sex differences regarding the proliferative response of human PAECs to the EH_{ITSN} expression, with PAECs of female donor possessing a higher proliferation rate compared with the PAECs of male donor,[29]

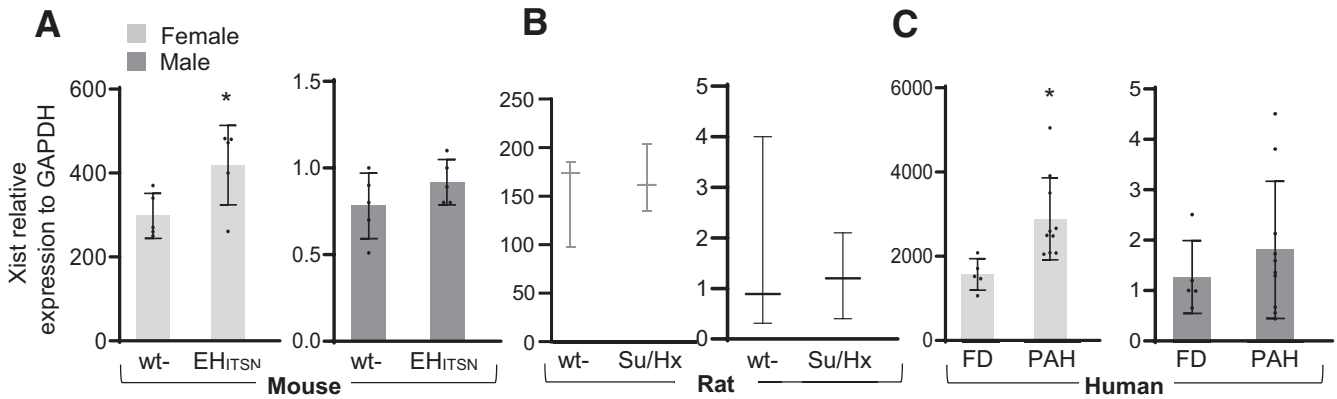

Figure 4 Expression of the long noncoding RNA (lncRNA)—Xist is increased in mouse and human female pulmonary arterial hypertension (PAH) lung tissue. Relative expression of lncRNA-Xist in the lung tissue of female and male EH_{ITSN}-$KO^{ITSN+/-}$ mice (**A**), Sugen5416 inhibitor/hypoxia (Su/Hx) rats (**B**), and human PAH patients (**C**) and the matching controls, as determined by real-time quantitative PCR analyses. At least nine mice and three rats per condition and RNA isolated form the lung tissue of 10 to 12 PAH subjects and five failed donors (FDs) for each human female and male were used in three independent experiments performed in triplicates. Human lung RNA samples (from Pulmonary Hypertension Breakthrough Initiative): idiopathic PAH female: 10 White, 8 not Hispanic, and 2 Hispanic or Latino (average age, 34.1 years; range, 15 to 56 years); idiopathic PAH male: 9 White, 1 Asian, 8 non-Hispanic, and 2 Hispanic or Latino (average age, 33.2 years; range, 7 to 61 years); FDs: 5 males, White non-Hispanic (average age, 31 years; range, 14 to 49 years); 5 females, White non-Hispanic (average age, 50 years; range, 33 to 60 years). Data represent means ± SD (**A**–**C**). *$P < 0.05$. GAPDH, glyceraldehyde-3-phosphate dehydrogenase; wt, wild type.

subsequent studies investigated whether the mouse PAECs show similar differences in their proliferative response to the expression of EH_{ITSN} protein fragment. To this end, a double bromodeoxyuridine (BrdU)/CD31 immunofluorescence was performed on lung sections of EH_{ITSN}-$KO^{ITSN+/-}$ male (Figure 5, A and B) and female (Figure 5, C and D) mice. Untreated $KO^{ITSN+/-}$ mice (Figure 5, E and F) and wt mice injected with the empty vector (Figure 5, G and H) served as controls. Imaging and morphometric analyses indicated no significant differences between the numbers of BrdU/CD31-positive PAECs between the female and male control mouse lung specimens, $KO^{ITSN+/-}$ mouse (female specimen shown) (Figure 5, E and F), or wt mouse (male specimen shown) (Figure 5, G and H), with less than two BrdU-positive ECs per pulmonary artery profile, on average (Figure 5I). However, the mouse lung sections of the EH_{ITSN}-transduced male and female $KO^{ITSN+/-}$ mice showed more CD31/BrdU-positive ECs per pulmonary artery profile, compared with controls. On average, four BrdU-positive cells per pulmonary artery profile for male specimens (Figure 5, A and B) and seven BrdU-positive ECs per pulmonary artery profile for female specimens (Figure 5, C and D) were detected. The EH_{ITSN} expression caused a 37% increase in the BrdU-positive female ECs compared with that in female wt controls (Figure 5I). The male PAECs showed a similar trend in their proliferative response to the expression of the EH_{ITSN}, but like the human PAECs, they were less responsive, with only 25% increase in their proliferation rate. Data are expressed as BrdU/CD31-positive ECs/vessel profile. These data demonstrate that the PAECs of the female EH_{ITSN}-$KO^{ITSN+/-}$ mice have a higher proliferation rate compared with the PAECs of the male EH_{ITSN}-$KO^{ITSN+/-}$ mice.

Up-Regulation of the lncRNA-Xist in Female PAH Specimens Modulates the Expression of Elk1, an X-Linked PAH Gene

Expression of Elk1 is up-regulated in the PAECs of PAH patients, with female PAECs showing a higher increase.[32] To further support this *in vitro* observation, the expression of Elk1 was investigated *in vivo*, in the lung tissue of the EH_{ITSN}-$KO^{ITSN+/-}$ mice and PAH patients, both males and females. As determined by qPCR, Elk1 was up-regulated in the lungs of female EH_{ITSN}-$KO^{ITSN+/-}$ mice (average values, 1.00 in female wt mice versus 1.293 in female EH_{ITSN}-$KO^{ITSN+/-}$ mice; $P < 0.0009$) (Figure 6A). In male mice, the average Elk1 values were 1.18 in wt mice versus 1.314 in EH_{ITSN}-$KO^{ITSN+/-}$ mice ($P < 0.006$). Elk1 up-regulation was recapitulated by the human PAH patients (Figure 6B). Notably, all female PAH RNA samples showed higher Elk1 expression than the female FD, consistent with Elk1 up-regulation as part of a common mechanism of female PAEC proliferation in PAH (average values, 1.042 in female FD versus 2.002 in female PAH; $P < 0.0001$). No significant change in Elk1 was detected in the male PAH samples versus male FD (1.25 in male FD versus 1.73 in male PAH; $P < 0.08$). However, like Xist, the range of Elk1 mRNA levels was wide, suggesting that up-regulation of Elk1 may cause increased proliferation of a subset of male PAECs, as well. Elk1 increase in male human $PAEC_{PAH}$ was not statistically significant, whereas in mice, the exogenous expression of the EH_{ITSN} explained the statistically significant increase in Elk1 levels. The qPCR analyses of Elk1 mRNA expression in the lung tissue of female and male Su/Hx rats indicated no significant change as compared to the corresponding wt rats (Figure 6C).

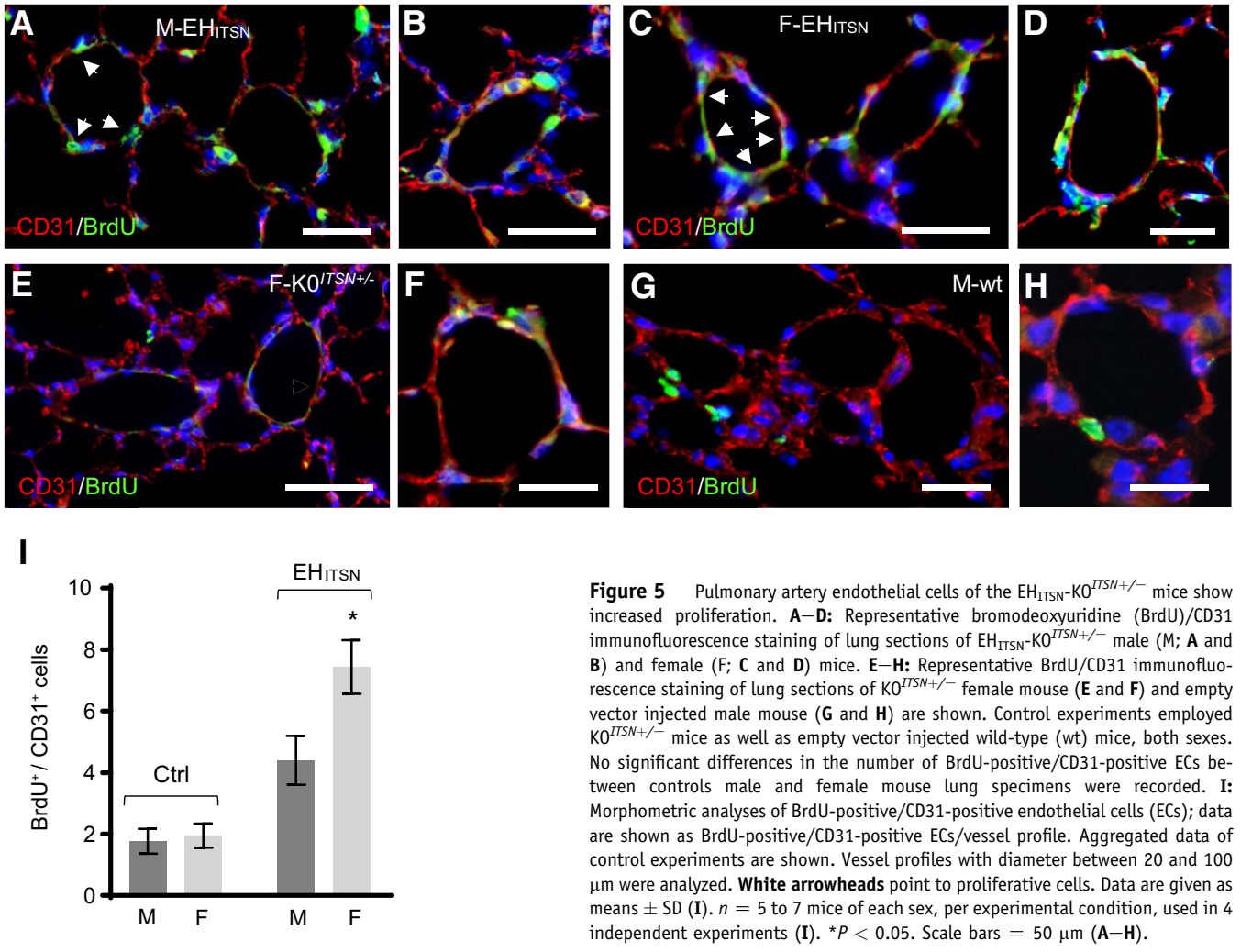

Figure 5 Pulmonary artery endothelial cells of the EH_{ITSN}-$KO^{ITSN+/-}$ mice show increased proliferation. **A**–**D:** Representative bromodeoxyuridine (BrdU)/CD31 immunofluorescence staining of lung sections of EH_{ITSN}-$KO^{ITSN+/-}$ male (M; **A** and **B**) and female (F; **C** and **D**) mice. **E**–**H:** Representative BrdU/CD31 immunofluorescence staining of lung sections of $KO^{ITSN+/-}$ female mouse (**E** and **F**) and empty vector injected male mouse (**G** and **H**) are shown. Control experiments employed $KO^{ITSN+/-}$ mice as well as empty vector injected wild-type (wt) mice, both sexes. No significant differences in the number of BrdU-positive/CD31-positive ECs between controls male and female mouse lung specimens were recorded. **I:** Morphometric analyses of BrdU-positive/CD31-positive endothelial cells (ECs); data are shown as BrdU-positive/CD31-positive ECs/vessel profile. Aggregated data of control experiments are shown. Vessel profiles with diameter between 20 and 100 μm were analyzed. **White arrowheads** point to proliferative cells. Data are given as means ± SD (**I**). $n = 5$ to 7 mice of each sex, per experimental condition, used in 4 independent experiments (**I**). $^*P < 0.05$. Scale bars = 50 μm (**A**–**H**).

Moreover, Western blot analyses of lung tissue showed increased expression of Elk1 protein level in female $PAEC_{PAH}$ and mouse lung lysates, as indicated (Figure 6D). No changes in Elk1 protein expression were detected in female versus male Su/Hx rats (Figure 6D). The findings strongly suggest that the aberrant expression of Xist in human female $PAEC_{PAH}$ and PAH lung tissue, as well as in the lungs of the EH_{ITSN}-$KD^{ITSN+/-}$ female mice, modulates Elk1 expression, an X-linked gene implicated in PAH pathogenesis.

Sex-Specific Increased Expression of Cyclin A Promotes Cell Cycle Progression and Hyperproliferation of Female $PAEC_{PAH}$

In proliferative cells, cell cycle regulatory proteins are often aberrantly expressed, resulting in abnormal cycling through the various phases of the cell cycle. The RNA sequencing of total RNA isolated from female and male $PAEC_{PAH}$ indicated that cyclin A1 and cyclin D2, two cell cycle regulatory proteins, are highly up-regulated in female $PAEC_{PAH}$. Cyclin A1 was up-regulated in the lungs of female EH_{ITSN}-$KO^{ITSN+/-}$ mice (Figure 7A); the $\log_2$ fold change values are indicated. Cyclin A1 is required for entry into the S and M phases of the cell cycle, whereas cyclin D2 promotes progression through G_1.[52] Moreover, the cyclin A1 has a putative binding site for Elk1, a transcription factor shown to contribute to cell cycle progression in a tissue- and cell-specific manner.[34,35] The cyclin A1 promoter (the region spanning −1040/−980 in human cyclin A1 and −980/−920 in mouse cyclin A1) contains the Elk1 consensus motif[34,53,54] (Figure 7B). The *cyclin D2* is a target of Elk1.[55] Moreover, the expression of cyclin A1 in synchronized cells was greater in female $PAEC_{PAH}$ compared with not only female and male $PAEC_{Ctrl}$, but also male $PAEC_{PAH}$ (Figure 7C). In the S phase, female $PAEC_{PAH}$ showed 2.57-fold increase in cyclin A1 expression and 1.6-fold increase in the G_2/M phase, compared with male $PAEC_{PAH}$ (Figure 7D). The increase of the cyclin A1 expression was also detected by qPCR analyses in the EH_{ITSN}-transduced $KO^{ITSN+/-}$ female mice, but not in

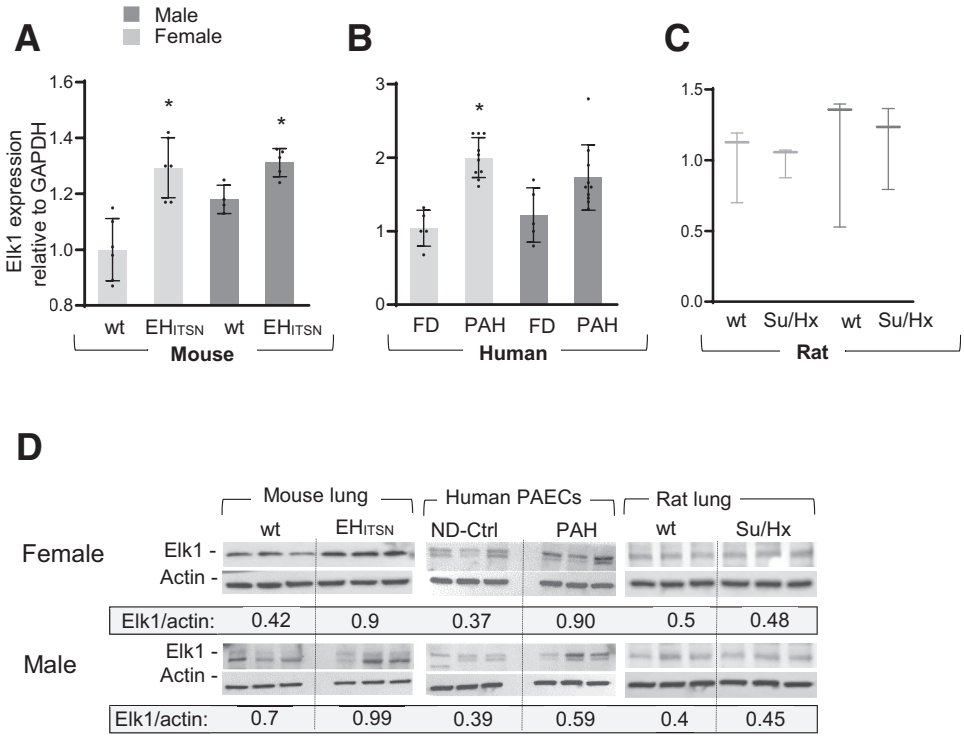

Figure 6 Relative expression of Elk1 in the lung of female and male EH_{ITSN}-$KO^{ITSN+/-}$ mice and human $PAEC_{PAH}$. **A**–**C:** Real-time quantitative PCR of mRNA isolated from female and male wild-type (wt) and EH_{ITSN}-$KO^{ITSN+/-}$ mouse lungs (**A**), 5 mice per experimental condition, 5 failed donors (FDs), and 10 human PAH lungs (**B**), and wt and Sugen5416 inhibitor/hypoxia (Su/Hx) rats (**C**), 3 rats per experimental condition. Data are representative of three independent experiments performed in triplicate. **D:** Western blot (WB) analyses of Elk1 protein expression in the lung lysates of female and male wt and EH_{ITSN}-$KO^{ITSN+/-}$ mice, three randomly selected PAEC lines of PAH patients and FD subjects, and wt and Su/Hx rats, as indicated. Identical detection conditions were used for WB analyses and electrochemiluminescence detection. Densitometry shows the average of Elk1/actin ratios in controls and PAH conditions. *P* value shown for EH_{ITSN}-$KO^{ITSN+/-}$ females and males versus the corresponding wt mice, and for PAH human female PAECs versus female ND-Ctrl cells; no significant differences were recorded for human PAH male PAECs versus ND-Ctrl male cells and for Su/Hx male and female rats versus the corresponding wt controls. Elk1 and actin immunoreactivities detected in the control samples and different experimental conditions (EH_{ITSN}, human $PAEC_{PAH}$, and Su/Hx rat), as indicated, are separated by **vertical lines**. Human PAEC lines (from Pulmonary Hypertension Breakthrough Initiative): idiopathic PAH: 5 White females (average age, 30.6 years; range, 16 to 47 years); 5 males (3 White, 2 Black) (average age, 48.8 years; range, 27 to 54 years); FDs: 3 White females (aged 36, 49, and 55 years); 2 White males and 1 of unknown race (aged 25, 20, and 30 years); all non-Hispanic. Data represent means ± SD (**A**–**C**). $n = 3$ independent experiments (**D**). $^*P < 0.05$. Elk1, ETS domain containing protein; GAPDH, glyceraldehyde-3-phosphate dehydrogenase; ND-Ctrl, nondisease controls; $PAEC_{PAH}$, pulmonary artery endothelial cells of pulmonary arterial hypertension patients.

the Su/Hx female rats (Figure 7, E and F). Thus, the sex-specific increase of the expression of cyclin A1 mRNA and of cyclin A1 protein in the S phase of the synchronized female $PAEC_{PAH}$ may be Elk1 mediated, strongly suggesting functional hyperproliferation.

Discussion

The findings presented herein provide evidence that targeted expression of the EH_{ITSN} in murine lungs generates a mouse model of PAH that closely recapitulates the human disease. The EH_{ITSN} is a result of granzyme B cleavage of ITSN under inflammatory conditions associated with PAH, and is present in the lungs of PAH animal models and human patients.[28,37] Morphologic and functional data demonstrated significant differences between female and male mice with regard to EH_{ITSN}-induced alterations in the RVSP, RV hypertrophy, and pulmonary artery remodeling. Consistent with the gendered paradox in PAH, male EH_{ITSN}-$KO^{ITSN+/-}$ mice, similar to human PAH male patients, showed greater RVSP and RV hypertrophy compared with female EH_{ITSN}-$KO^{ITSN+/-}$ mice. Previous studies suggest that sex hormones directly affect the cardiac function.[2] In humans, higher circulating estrogen levels are associated with better RV systolic function (strongly tied to survival in PAH), whereas higher levels of androgens are associated with greater RV mass and volume.[56] RV hypertrophy and failure is the proximate cause of death in PAH.[2] Despite significant effort, the reliance on sex hormones and their metabolites has not solved the sex paradox in PAH. Estrogen-independent mechanisms, like regulatory T-cell dysfunction,[57–59] vascular mitochondria abnormalities and inflammasome activation,[60] abnormal Xist expression, leading to deficient X-Chr inactivation, and aberrant expression of X-linked PAH genes, may be relevant to better understand the so-called sex paradox. The X-chromosome has the greatest density of immunity-related genes, and thus females, with two

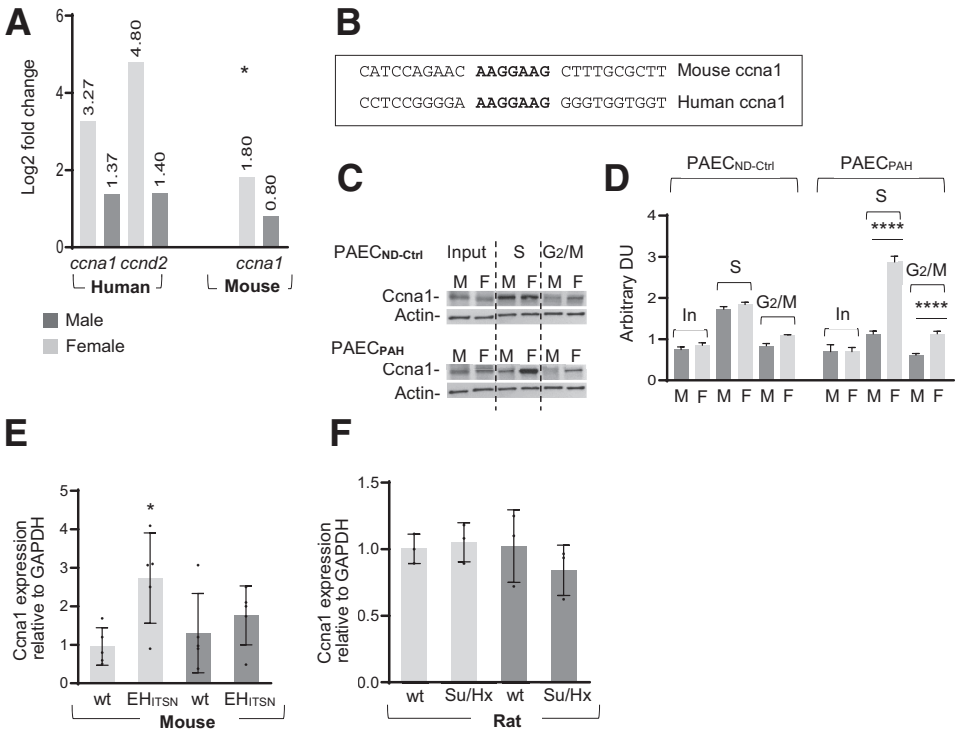

Figure 7 Sex-specific increased expression of cyclin A *(ccna1)* promotes cell cycle progression and hyperproliferation of female (F) $PAEC_{PAH}$. **A:** The RNA sequencing of RNA isolated from female and male (M), $PAEC_{PAH}$, and lung tissue of EH_{ITSN}-$KO^{ITSN+/-}$ mice shows log_2 fold change in cyclin A1 and cyclin D2 levels. Human female and male $PAEC_{ND-Ctrl}$ and wild-type (wt) mice served as controls. The cyclin D2 expression does not show significant changes in EH_{ITSN}-$KO^{ITSN+/-}$ mouse lung; false-discovery rate–adjusted *P* value. **B:** The murine and human cyclin A1 promoters, indicating the Elk1 binding motif (bold), conserved in mouse and human. Elk1 binds to sequences centered on the GGA trinucleotide motif (*http://www.ensembl.org/index.html*, last accessed January 19, 2020). **C:** Expression of cyclin A1 in synchronized male and female $PAEC_{ND-Ctrl}$ and $PAEC_{PAH}$. Cells were synchronized using 2 μg/mL aphidicolin (G_1/S phase) and 0.1 μg/mL nocodazole (G_2/M phase). The **dotted vertical lines** separate the ccna1 and actin immunoreactivities in the Input (In; not synchronized cells), S, and G_2/M phases of the cell cycle. **D:** The histogram shows the ratio cyclin A1/actin, as determined by densitometry of three representative X-ray films, demonstrating the sex-specific increase in cyclin A1 expression in the S and G_2/M phases of the synchronized $PAEC_{PAH}$. **E** and **F:** Real-time quantitative PCR of mRNA isolated from EH_{ITSN}-$KO^{ITSN+/-}$ mice (**E**) and Sugen5416 inhibitor/hypoxia (Su/Hx) rats (**F**). The wt animals served as controls. Data are shown as means ± SD and are representative for 3 independent experiments performed in triplicate (**D**–**F**). $n = 5$ mice per experimental condition (**E**); $n = 3$ rats per experimental condition (**F**). $^*P < 0.05$, $^{****}P < 0.0001$. DU, densitometric units; Elk1, ETS domain containing protein; GAPDH, glyceraldehyde-3-phosphate dehydrogenase; ND-Ctrl, nondisease controls; $PAEC_{PAH}$, pulmonary artery endothelial cells of pulmonary arterial hypertension patients.

X-chromosomes, have an immunologic advantage over males (XY). This indicates that sex-mediated differences in immune function may affect disease development, progression, and severity, and contribute to the female survival benefit. How sex-based differences in immunity impact PAH remains to be investigated.

The p38/Elk1/c-Fos signaling, accountable for these changes, is more activated in EH_{ITSN}-$KO^{ITSN+/-}$ female mice compared with males, leading to increased PAEC proliferative response and more severe lung phenotype, characterized by severe vascular arteriopathy, including complex plexiform lesions similar to human disease.[28] Recently published data demonstrate that the expression of the EH_{ITSN} in PAECs upregulates the expression of the lncRNA-Xist in female compared with nontransfected female cells, leading to aberrant expression of the transcription factor Elk1, an X-linked gene. Consistent with these data, Xist, a lncRNA that mediates X-Chr inactivation essential for equalizing the expression of X-linked genes between females and males,[9] is significantly up-regulated in the lung tissue of EH_{ITSN}-transduced $KO^{ITSN+/-}$ female mice, leading to sex-specific regulation of Elk1. Increased Elk1 expression leads to sex differences in one of its target genes, the cell cycle regulatory protein cyclin A1, a gene not encoded on the X-chromosome. The expression changes are small, but as shown, they are associated with large phenotypic effects on the murine lung.

Important issues regarding the genetics of sex differences also relate to the preclinical work involving experimental animal model(s) used as critical tools to investigate human disease. The laboratory mouse has become the preferred model organism for studying and validating the genetics of sex differences for human conditions, as well as identifying previously unsuspected disease-associated genes.[61,62] Relevant to this study, the X-linked genes associated to PAH are shared by human and mouse.[32] Dysregulation of Xist can result in genes escaping inactivation or reactivation in female cells.[63] Thus, aberrant expression of the lncRNA-Xist may affect the expression of genes not only on mouse X-chromosome but also on human X-chromosome, and documented to be involved in PAH pathogenesis.[13–28]

Sex differences are widespread in many human diseases. However, the molecular basis and the mechanisms driving

these sex differences are poorly understood. The failure to include the sex chromosomes (XX in females and XY in males) in genome-wide association studies, to account for sex as variable in targeted genetic analyses, for X-chromosome dosage compensation of X-linked gene expression and for up-regulation or inactivation of X-chromosome−specific genes may all be related to differential gene expression across the sexes and, thus, important considerations for sex-specific disease risk. Previous reports have identified several X-chromosome−linked genes, outside of the pseudoautosomal region with aberrant protein expression in PAH animal models and human patients.[64] However, no studies have addressed the deviant expression of these genes in female PAH compared with male PAH and their role in the increased incidence of PAH in females compared with males. Altered expression of X-linked genes is also observed in female-biased autoimmune disorders and mouse models of autoimmunity.[65] The current study, using total RNA isolated from human male and female PAH lung tissue, demonstrates that similar to the EH_{ITSN}-$KO^{ITSN+/-}$ mice, the human female PAH samples show aberrant expression of the lncRNA-Xist, which. This, in turn, drives differential sex-specific regulation of the X-linked gene Elk1 and its target cyclin A1. These molecular events are not detected in the Su/Hx female rat, a widely used and generally accepted animal model of PAH that develops severe plexiform arteriopathy,[45] but has no significant differences between female and male with regard to Su/Hx-induced alterations in the RVSP, RV hypertrophy, or pulmonary artery remodeling.[8]

The current finding is consistent with published literature suggesting that in this rat, the mechanism of severe angioproliferative PAH occurs via VEGF-C and VEGF-D signaling through VEGF receptor 3.[66] VEGF receptor 3 is a downstream target of p38 kinase reported to be activated in this experimental animal model of PAH and to regulate cell proliferation and cell cycle progression by increasing the mRNA and protein levels of cyclin D1.[67−70] Moreover, lack of changes in Elk1 expression in the Su/Hx rats compared with controls does not rule out the possibility that Elk1 activation, induced by p38 signaling, activated in these rats and involved in the formation of plexiform lesions in the EH_{ITSN}-$K0^{ITSN+/-}$ mice,[28,37,69] might be a molecular determinant of the Su/Hx rat PAH phenotype.

Although this study introduces the lncRNA-Xist as a critical determinant of female susceptibility to PAH and a specific factor driving the X-Chr influence in PAH, a protective role of the chromosome Y in PAH has been recently reported.[71,72] Using a murine model in which sex chromosomes are independent of gonadal sex [XX and XY mice with testes (males) and XX and XY mice with ovaries (females)], Umar et al[71] have found that XY mice, irrespective of the gonadal sex, developed less severe PAH compared with XX mice; several chromosome Y genes expressed in the lung (*Ddx3y*, *Eif2s3y*, *Kdm5d*, and *Uty*) with potential impact on cell proliferation, apoptosis, and epigenetic regulation support a protective role of the chromosome Y in PAH. The expression of three of these genes (*Ddx3y*, *Eif2s3y*, and *Uty)* is also down-regulated in the lung of the EH_{ITSN}-$KO^{ITSN+/-}$ male mice (S. Predescu, unpublished data). The protective role of the chromosome Y in PAH is also supported by recent chromatin immunoprecipitation studies using male fibroblast cell lines; the endogenous chromosome Y gene *Sry,* a member of the Sry-like box family of transcription factors expressed exclusively in males, bound to and positively regulates the bone morphogenetic protein receptor type 2 promoter. As reduced expression of the bone morphogenetic protein receptor type 2 is detrimental in PAH, the positive regulation of bone morphogenetic protein receptor type 2 by *Sry* may contribute to the protective role of chromosome Y in PAH.[72]

Several experimental rodent models of PAH developed over the past 15 to 20 years demonstrate a female bias with regard to disease susceptibility or severity and have allowed for a better understanding of the effects of sex and sex hormones on disease development. Relevant to mention herein are the $miR214^{-/-}$ + Su/Hx rats that show RV hypertrophy in males with no difference in the RVSP or pulmonary artery remodeling.[73] Greater pulmonary artery resistance and RV hypertrophy, lower cardiac index, and higher left ventricular and arterial stiffness, most likely due to elevated aldosterone level, were detected by Cyp2c44 disruption and hypoxia exposure in female but not male mice.[74] Athymic female *rnu/rnu* rats, lacking regulatory T cells, treated with SU5416 or chronic hypoxia develop more severe pulmonary hypertension than males, suggesting that females are especially reliant on the normal regulatory T-cell function to counteract the effects of pulmonary vascular injury leading to pulmonary hypertension.[58] As with any other human disease, the animal models of PAH are not perfect equivalents of human physiology.

Our study has some limitations. Although it is a robust study, we performed this translational approach in a relatively small number of male and female PAH patients, with a clear finding that the lncRNA-Xist is up-regulated in the PAECs and the lungs of female PAH patients compared with female specimen used as controls, leading to sex-specific modulation of the X-linked PAH gene Elk1. However, because of small sample size and clinical heterogeneity, this finding needs to be confirmed in a larger cohort of patients. Another limitation may be the existence of other drivers of cell cycle progression, such as repression of Kruppel like factor 2, a Xist target,[29] that, in turn, can affect other target genes, such as *cyclin kinase 1a* and *2b* or some X-Chr-linked (*Timp1, Apln*, and *Ace*),[75] potentially implicated in PAEC proliferation and blood pressure regulation. Also, in non−small-cell lung cancer, the lncRNA just proximal to Xist, an activator of Xist on X-Chr, up-regulates the cyclin D2, affecting cell cycle progression.[76] Finally, the use of the Su/Hx rat model as the experimental control instead of a mouse model may be another limitation. The

Su/Hx rat is the standard in the field as it recapitulates clinical pathology better than any other rodent model reported so far, with no significant differences between female and male with regard to Su/Hx-induced alterations in the RVSP, RV hypertrophy, or pulmonary artery remodeling.[8] In the Su/Hx murine model, the range of vesicular lesions and severity of the hemodynamics and RV changes are less severe compared with the rat counterpart and, more important, only male mice have been used.[77,78]

In sum, the data reported herein strongly suggest that the EH_{ITSN}-triggered up-regulation of the lncRNA-Xist in females, leading to altered expression of X-linked genes associated with PAH condition, could underlie a significant fraction of increased incidence of PAH in females compared with males. The findings strongly suggest that the EH_{ITSN} expression triggers sex differences in PAH by: up-regulation above basal levels of lncRNA-Xist and some of its target genes in females compared with males; random up-regulation of several X-linked genes already implicated in PAH pathogenesis (apelin, tissue inhibitor of metalloproteinases 1, angiotensin-converting enzyme, Elk1, and androgen receptor); as well as up-regulation of Xist-controlled proliferation pathways. Thus, these studies identify Xist as a critical determinant of female susceptibility to PAH.

Acknowledgments

We thank Drs. Serpil Erzurum and Suzy Comhair (Lerner Research Institute, Cleveland Clinic Lerner College of Medicine Cleveland Clinic; HL60917) and Pulmonary Hypertension Breakthrough Initiative for providing the pulmonary artery endothelial cells isolated from pulmonary arterial hypertension patients and nondisease controls; Dr. Estefania Oliveros Soles (Rush University Medical Center) for interpreting of murine echocardiography data; and the NuSeq Core Facility (Northwestern University) for the RNA sequencing studies.

References

1. Batton KA, Austin CO, Bruno KA, Burger CD, Shapiro BP, Fairweather D: Sex differences in pulmonary arterial hypertension: role of infection and autoimmunity in the pathogenesis of disease. Biol Sex Differences 2018, 9:15
2. Hester J, Ventetuolo C, Lahm T: Sex, gender, and sex hormones in pulmonary hypertension and right ventricular failure. Compr Physiol 2019, 10:125−170
3. Morrell NW: Pulmonary hypertension due to BMPR2 mutation: a new paradigm for tissue remodeling? Proc Am Thorac Soc 2006, 3:680−686
4. Lahm T, Tuder RM, Petrache I: Progress in solving the sex hormone paradox in pulmonary hypertension. Am J Physiol Lung Cell Mol Physiol 2014, 307:L7−L26
5. Austin ED, Loyd JE, Phillips JA 3rd: Genetics of pulmonary arterial hypertension. Semin Respir Crit Care Med 2009, 30:386−398
6. Dempsie Y, MacLean MR: The influence of gender on the development of pulmonary arterial hypertension. Exp Physiol 2013, 98: 1257−1261
7. Austin ED, Lahm T, West J, Tofovic SP, Johansen AK, Maclean MR, Alzoubi A, Oka M: Gender, sex hormones and pulmonary hypertension. Pulm Circ 2013, 3:294−314
8. Frump AL, Goss KN, Vayl A, Albrecht M, Fisher A, Tursunova R, Fierst J, Whitson J, Cucci AR, Brown MB, Lahm T: Estradiol improves right ventricular function in rats with severe angioproliferative pulmonary hypertension: effects of endogenous and exogenous sex hormones. Am J Physiol Lung Cell Mol Physiol 2015, 308:L873−L890
9. Yang Z, Jiang X, Jiang X, Zhao H: X-inactive-specific transcript: a long noncoding RNA with complex roles in human cancers. Gene 2018, 679:28−35
10. Schurz H, Salie M, Tromp G, Hoal EG, Kinnear CJ, Moller M: The X chromosome and sex-specific effects in infectious disease susceptibility. Hum Genomics 2019, 13:2
11. Sahakyan A, Yang Y, Plath K: The role of Xist in X-chromosome dosage compensation. Trends Cell Biol 2018, 28:999−1013
12. Lessing D, Anguera MC, Lee JT: X chromosome inactivation and epigenetic responses to cellular reprogramming. Annu Rev Genomics Hum Genet 2013, 14:85−110
13. Brash L, Barnes GD, Brewis MJ, Church AC, Gibbs SJ, Howard L, Jayasekera G, Johnson MK, McGlinchey N, Onorato J, Simpson J, Stirrat C, Thomson S, Watson G, Wilkins MR, Xu C, Welsh DJ, Newby DE, Peacock AJ: Short-term hemodynamic effects of apelin in patients with pulmonary arterial hypertension. JACC Basic Transl Sci 2018, 3:176−186
14. Yang P, Read C, Kuc RE, Buonincontri G, Southwood M, Torella R, Upton PD, Crosby A, Sawiak SJ, Carpenter TA, Glen RC, Morrell NW, Maguire JJ, Davenport AP: Elabela/toddler is an endogenous agonist of the apelin APJ receptor in the adult cardiovascular system, and exogenous administration of the peptide compensates for the downregulation of its expression in pulmonary arterial hypertension. Circulation 2017, 135:1160−1173
15. Yang P, Read C, Kuc RE, Nyimanu D, Williams TL, Crosby A, Buonincontri G, Southwood M, Sawiak SJ, Glen RC, Morrell NW, Davenport AP, Maguire JJ: A novel cyclic biased agonist of the apelin receptor, MM07, is disease modifying in the rat monocrotaline model of pulmonary arterial hypertension. Br J Pharmacol 2019, 176:1206−1221
16. Tiede SL, Wassenberg M, Christ K, Schermuly RT, Seeger W, Grimminger F, Ghofrani HA, Gall H: Biomarkers of tissue remodeling predict survival in patients with pulmonary hypertension. Int J Cardiol 2016, 223:821−826
17. Chelladurai P, Seeger W, Pullamsetti SS: Matrix metalloproteinases and their inhibitors in pulmonary hypertension. Eur Respir J 2012, 40: 766−782
18. Wang XM, Shi K, Li JJ, Chen TT, Guo YH, Liu YL, Yang YF, Yang S: Effects of angiotensin II intervention on MMP-2, MMP-9, TIMP-1, and collagen expression in rats with pulmonary hypertension. Genet Mol Res 2015, 14:1707−1717
19. Boucherat O, Chabot S, Paulin R, Trinh I, Bourgeois A, Potus F, Lampron MC, Lambert C, Breuils-Bonnet S, Nadeau V, Paradis R, Goncharova EA, Provencher S, Bonnet S: HDAC6: a novel histone deacetylase implicated in pulmonary arterial hypertension. Sci Rep 2017, 7:4546
20. Hemnes AR, Rathinasabapathy A, Austin EA, Brittain EL, Carrier EJ, Chen X, Fessel JP, Fike CD, Fong P, Fortune N, Gerszten RE, Johnson JA, Kaplowitz M, Newman JH, Piana R, Pugh ME, Rice TW, Robbins IM, Wheeler L, Yu C, Loyd JE, West J: A potential therapeutic role for angiotensin-converting enzyme 2 in human pulmonary arterial hypertension. Eur Respir J 2018, 51:1702638
21. Li G, Liu Y, Zhu Y, Liu A, Xu Y, Li X, Li Z, Su J, Sun L: ACE2 activation confers endothelial protection and attenuates neointimal lesions in prevention of severe pulmonary arterial hypertension in rats. Lung 2013, 191:327−336
22. Huang L, Li L, Hu E, Chen G, Meng X, Xiong C, He J: Potential biomarkers and targets in reversibility of pulmonary arterial hypertension secondary to congenital heart disease: an explorative study. Pulm Circ 2018, 8. 2045893218755987

23. Hirashiki A, Adachi S, Nakano Y, Kamimura Y, Ogo T, Nakanishi N, Morisaki T, Morisaki H, Shimizu A, Toba K, Murohara T, Kondo T: Left main coronary artery compression by a dilated main pulmonary artery and left coronary sinus of Valsalva aneurysm in a patient with heritable pulmonary arterial hypertension and FLNA mutation. Pulm Circ 2017, 7:734−740
24. Barnes JW, Tian L, Heresi GA, Farver CF, Asosingh K, Comhair SA, Aulak KS, Dweik RA: O-linked beta-N-acetylglucosamine transferase directs cell proliferation in idiopathic pulmonary arterial hypertension. Circulation 2015, 131:1260−1268
25. Elinoff JM, Rame JE, Forfia PR, Hall MK, Sun J, Gharib AM, Abd-Elmoniem K, Graninger G, Harper B, Danner RL, Solomon MA: A pilot study of the effect of spironolactone therapy on exercise capacity and endothelial dysfunction in pulmonary arterial hypertension: study protocol for a randomized controlled trial. Trials 2013, 14:91
26. Ghouleh IA, Sahoo S, Meijles DN, Amaral JH, de Jesus DS, Sembrat J, Rojas M, Goncharov DA, Goncharova EA, Pagano PJ: Endothelial Nox1 oxidase assembly in human pulmonary arterial hypertension; driver of Gremlin1-mediated proliferation. Clin Sci 2017, 131:2019−2035
27. Hood KY, Montezano AC, Harvey AP, Nilsen M, MacLean MR, Touyz RM: Nicotinamide adenine dinucleotide phosphate oxidase-mediated redox signaling and vascular remodeling by 16alpha-hydroxyestrone in human pulmonary artery cells: implications in pulmonary arterial hypertension. Hypertension 2016, 68:796−808
28. Patel M, Predescu D, Bardita C, Chen J, Jeganathan N, Pritchard M, DiBartolo S, Machado R, Predescu S: Modulation of intersectin-1s lung expression induces obliterative remodeling and severe plexiform arteriopathy in the murine pulmonary vascular bed. Am J Pathol 2017, 187:528−542
29. Qin S, Predescu DN, Patel M, Drazkowski P, Ganesh B, Predescu SA: Sex differences in the proliferation of pulmonary artery endothelial cells: implications for plexiform arteriopathy. J Cell Sci 2020, 133:jcs237776
30. van de Veerdonk MC, Kind T, Marcus JT, Mauritz GJ, Heymans MW, Bogaard HJ, Boonstra A, Marques KM, Westerhof N, Vonk-Noordegraaf A: Progressive right ventricular dysfunction in patients with pulmonary arterial hypertension responding to therapy. J Am Coll Cardiol 2011, 58:2511−2519
31. Carman BL, Predescu DN, Machado R, Predescu SA: Plexiform arteriopathy in rodent models of pulmonary arterial hypertension. Am J Pathol 2019, 189:1133−1144
32. Qin S, Predescu DN, Patel M, Drazkowski P, Ganesh B, Predescu S: Pulmonary artery endothelial cells are sex dimorphic in their proliferative potential: implications for plexiform arteriopathy. J Cell Sci 2020, [Epub ahead of print] doi: 10.1242/jcs.237776
33. Weiss A, Neubauer MC, Yerabolu D, Kojonazarov B, Schlueter BC, Neubert L, Jonigk D, Baal N, Ruppert C, Dorfmuller P, Pullamsetti SS, Weissmann N, Ghofrani HA, Grimminger F, Seeger W, Schermuly RT: Targeting cyclin-dependent kinases for the treatment of pulmonary arterial hypertension. Nat Commun 2019, 10:2204
34. Boros J, Donaldson IJ, O'Donnell A, Odrowaz ZA, Zeef L, Lupien M, Meyer CA, Liu XS, Brown M, Sharrocks AD: Elucidation of the ELK1 target gene network reveals a role in the coordinate regulation of core components of the gene regulation machinery. Genome Res 2009, 19:1963−1973
35. Yordy JS, Muise-Helmericks RC: Signal transduction and the Ets family of transcription factors. Oncogene 2000, 19:6503−6513
36. Comhair SA, Xu W, Mavrakis L, Aldred MA, Asosingh K, Erzurum SC: Human primary lung endothelial cells in culture. Am J Respir Cell Mol Biol 2012, 46:723−730
37. Patel M, Predescu D, Tandon R, Bardita C, Pogoriler J, Bhorade S, Wang M, Comhair S, Hemnes AR, Chen J, Machado R, Husain A, Erzurum S, Predescu S: A novel p38 mitogen-activated protein kinase/Elk-1 transcription factor-dependent molecular mechanism underlying abnormal endothelial cell proliferation in plexogenic pulmonary arterial hypertension. J Biol Chem 2013, 288: 25701−25716
38. Bardita C, Predescu D, Justice MJ, Petrache I, Predescu S: In vivo knockdown of intersectin-1s alters endothelial cell phenotype and causes microvascular remodeling in the mouse lungs. Apoptosis 2013, 18:57−76
39. Predescu DN, Neamu R, Bardita C, Wang M, Predescu SA: Impaired caveolae function and upregulation of alternative endocytic pathways induced by experimental modulation of intersectin-1s expression in mouse lung endothelium. Biochem Res Int 2012, 2012:672705
40. de Beer T, Carter RE, Lobel-Rice KE, Sorkin A, Overduin M: Structure and Asn-Pro-Phe binding pocket of the Eps15 homology domain. Science 1998, 281:1357−1360
41. Tschanz SA, Burri PH, Weibel ER: A simple tool for stereological assessment of digital images: the STEPanizer. J Microsc 2011, 243:47−59
42. Stacher E, Graham BB, Hunt JM, Gandjeva A, Groshong SD, McLaughlin VV, Jessup M, Grizzle WE, Aldred MA, Cool CD, Tuder RM: Modern age pathology of pulmonary arterial hypertension. Am J Respir Crit Care Med 2012, 186:261−272
43. Tuder RM, Marecki JC, Richter A, Fijalkowska I, Flores S: Pathology of pulmonary hypertension. Clin Chest Med 2007, 28:23−42. vii
44. Tuder RM, Groves B, Badesch DB, Voelkel NF: Exuberant endothelial cell growth and elements of inflammation are present in plexiform lesions of pulmonary hypertension. Am J Pathol 1994, 144:275−285
45. Abe K, Toba M, Alzoubi A, Ito M, Fagan KA, Cool CD, Voelkel NF, McMurtry IF, Oka M: Formation of plexiform lesions in experimental severe pulmonary arterial hypertension. Circulation 2010, 121: 2747−2754
46. Dobin A, Davis CA, Schlesinger F, Drenkow J, Zaleski C, Jha S, Batut P, Chaisson M, Gingeras TR: STAR: ultrafast universal RNA-seq aligner. Bioinformatics 2013, 29:15−21
47. Anders S, Pyl PT, Huber W: HTSeq–a Python framework to work with high-throughput sequencing data. Bioinformatics 2015, 31: 166−169
48. Ewels P, Magnusson M, Lundin S, Kaller M: MultiQC: summarize analysis results for multiple tools and samples in a single report. Bioinformatics 2016, 32:3047−3048
49. Love MI, Huber W, Anders S: Moderated estimation of fold change and dispersion for RNA-seq data with DESeq2. Genome Biol 2014, 15:550
50. Zhou Y, Zhou B, Pache L, Chang M, Khodabakhshi AH, Tanaseichuk O, Benner C, Chanda SK: Metascape provides a biologist-oriented resource for the analysis of systems-level datasets. Nat Commun 2019, 10:1523
51. Jacobs W, van de Veerdonk MC, Trip P, de Man F, Heymans MW, Marcus JT, Kawut SM, Bogaard HJ, Boonstra A, Vonk Noordegraaf A: The right ventricle explains sex differences in survival in idiopathic pulmonary arterial hypertension. Chest 2014, 145:1230−1236
52. Brooks AR, Shiffman D, Chan CS, Brooks EE, Milner PG: Functional analysis of the human cyclin D2 and cyclin D3 promoters. J Biol Chem 1996, 271:9090−9099
53. Shore P, Sharrocks AD: The ETS-domain transcription factors Elk-1 and SAP-1 exhibit differential DNA binding specificities. Nucleic Acids Res 1995, 23:4698−4706
54. Katabami M, Donninger H, Hommura F, Leaner VD, Kinoshita I, Chick JF, Birrer MJ: Cyclin A is a c-Jun target gene and is necessary for c-Jun-induced anchorage-independent growth in RAT1a cells. J Biol Chem 2005, 280:16728−16738
55. Shukla S, Gupta S: Apigenin-induced cell cycle arrest is mediated by modulation of MAPK, PI3K-Akt, and loss of cyclin D1 associated retinoblastoma dephosphorylation in human prostate cancer cells. Cell Cycle 2007, 6:1102−1114
56. Ventetuolo CE, Ouyang P, Bluemke DA, Tandri H, Barr RG, Bagiella E, Cappola AR, Bristow MR, Johnson C, Kronmal RA, Kizer JR, Lima JA, Kawut SM: Sex hormones are associated with right ventricular structure and function: the MESA-right ventricle study. Am J Respir Crit Care Med 2011, 183:659−667
57. Huertas A, Phan C, Bordenave J, Tu L, Thuillet R, Le Hiress M, Avouac J, Tamura Y, Allanore Y, Jovan R, Sitbon O, Guignabert C,

Humbert M: Regulatory T cell dysfunction in idiopathic, heritable and connective tissue-associated pulmonary arterial hypertension. Chest 2016, 149:1482–1493
58. Tamosiuniene R, Manouvakhova O, Mesange P, Saito T, Qian J, Sanyal M, Lin YC, Nguyen LP, Luria A, Tu AB, Sante JM, Rabinovitch M, Fitzgerald DJ, Graham BB, Habtezion A, Voelkel NF, Aurelian L, Nicolls MR: Dominant role for regulatory T cells in protecting females against pulmonary hypertension. Circ Res 2018, 122:1689–1702
59. Taraseviciene-Stewart L, Nicolls MR, Kraskauskas D, Scerbavicius R, Burns N, Cool C, Wood K, Parr JE, Boackle SA, Voelkel NF: Absence of T cells confers increased pulmonary arterial hypertension and vascular remodeling. Am J Respir Crit Care Med 2007, 175:1280–1289
60. Sutendra G, Michelakis ED: The metabolic basis of pulmonary arterial hypertension. Cell Metab 2014, 19:558–573
61. Karp NA, Mason J, Beaudet AL, Benjamini Y, Bower L, Braun RE, et al: Prevalence of sexual dimorphism in mammalian phenotypic traits. Nat Communications 2017, 8:15475
62. Meehan TF, Conte N, West DB, Jacobsen JO, Mason J, Warren J, et al: Disease model discovery from 3,328 gene knockouts by The International Mouse Phenotyping Consortium. Nat Genet 2017, 49: 1231–1238
63. Vacca M, Della Ragione F, Scalabri F, D'Esposito M: X inactivation and reactivation in X-linked diseases. Semin Cell Dev Biol 2016, 56: 78–87
64. Aldred MA, Comhair SA, Varella-Garcia M, Asosingh K, Xu W, Noon GP, Thistlethwaite PA, Tuder RM, Erzurum SC, Geraci MW, Coldren CD: Somatic chromosome abnormalities in the lungs of patients with pulmonary arterial hypertension. Am J Respir Crit Care Med 2010, 182:1153–1160
65. Libert C, Dejager L, Pinheiro I: The X chromosome in immune functions: when a chromosome makes the difference. Nat Rev Immunol 2010, 10:594–604
66. Al-Husseini A, Kraskauskas D, Mezzaroma E, Nordio A, Farkas D, Drake JI, Abbate A, Felty Q, Voelkel NF: Vascular endothelial growth factor receptor 3 signaling contributes to angioobliterative pulmonary hypertension. Pulm Circ 2015, 5: 101–116
67. Feng Y, Hu J, Ma J, Feng K, Zhang X, Yang S, Wang W, Zhang J, Zhang Y: RNAi-mediated silencing of VEGF-C inhibits non-small cell lung cancer progression by simultaneously down-regulating the CXCR4, CCR7, VEGFR-2 and VEGFR-3-dependent axes-induced ERK, p38 and AKT signalling pathways. Eur J Cancer 2011, 47:2353–2363
68. Hu J, Cheng Y, Li Y, Jin Z, Pan Y, Liu G, Fu S, Zhang Y, Feng K, Feng Y: microRNA-128 plays a critical role in human non-small cell lung cancer tumourigenesis, angiogenesis and lymphangiogenesis by directly targeting vascular endothelial growth factor-C. Eur J Cancer 2014, 50:2336–2350
69. Rafikova O, Williams ER, McBride ML, Zemskova M, Srivastava A, Nair V, Desai AA, Langlais PR, Zemskov E, Simon M, Mandarino LJ, Rafikov R: Hemolysis-induced lung vascular leakage contributes to the development of pulmonary hypertension. Am J Respir Cell Mol Biol 2018, 59:334–345
70. Kodama M, Kitadai Y, Tanaka M, Kuwai T, Tanaka S, Oue N, Yasui W, Chayama K: Vascular endothelial growth factor C stimulates progression of human gastric cancer via both autocrine and paracrine mechanisms. Clin Cancer Res 2008, 14:7205–7214
71. Umar S, Cunningham CM, Itoh Y, Moazeni S, Vaillancourt M, Sarji S, Centala A, Arnold AP, Eghbali M: The Y chromosome plays a protective role in experimental hypoxic pulmonary hypertension. Am J Respir Crit Care Med 2018, 197:952–955
72. Yan L, Cogan JD, Hedges LK, Nunley B, Hamid R, Austin ED: The Y chromosome regulates BMPR2 expression via SRY: a possible reason "why" fewer males develop pulmonary arterial hypertension. Am J Respir Crit Care Med 2018, 198:1581–1583
73. Stevens HC, Deng L, Grant JS, Pinel K, Thomas M, Morrell NW, MacLean MR, Baker AH, Denby L: Regulation and function of miR-214 in pulmonary arterial hypertension. Pulm Circ 2016, 6: 109–117
74. Yang YM, Yuan H, Edwards JG, Skayian Y, Ochani K, Miller EJ, Sehgal PB: Deletion of STAT5a/b in vascular smooth muscle abrogates the male bias in hypoxic pulmonary hypertension in mice: implications in the human disease. Mol Med 2015, 20: 625–638
75. Zhang P, Kawakami H, Liu W, Zeng X, Strebhardt K, Tao K, Huang S, Sinicrope FA: Targeting CDK1 and MEK/ERK overcomes apoptotic resistance in BRAF-mutant human colorectal cancer. Mol Cancer Res 2018, 16:378–389
76. Nagel S, Pommerenke C, Meyer C, Kaufmann M, Drexler HG, MacLeod RA: Deregulation of polycomb repressor complex 1 modifier AUTS2 in T-cell leukemia. Oncotarget 2016, 7:45398–45413
77. de Jesus Perez VA: Molecular pathogenesis and current pathology of pulmonary hypertension. Heart Fail Rev 2016, 21:239–257
78. Vitali SH, Hansmann G, Rose C, Fernandez-Gonzalez A, Scheid A, Mitsialis SA, Kourembanas S: The Sugen 5416/hypoxia mouse model of pulmonary hypertension revisited: long-term follow-up. Pulm Circ 2014, 4:619–629